PREDICTION OF SLIDING RESISTANCE ON ASPHALT PAVEMENT SURFACE DUE TO FREEZING OF SODIUM CHLORIDE SOLUTION

A. Fujimoto, H. Watanabe & T. Fukuhara
University of Fukui, Fukui, Japan
afujimot@u-fukui.ac.jp

ABSTRACT

We developed a coupled heat and mass balance model (HMB model) for determining the skid resistance *BPN* for snow/ice (S/I) conditions on a road surface. The reliability of the HMB model was examined by comparison with the pavement temperature, the temperature and mass ice content of the ice-NaCl solution mixture (or ice-fresh water one) on the road surface, the salt concentration and the *BPN* value obtained from a laboratory experiment.

We have concluded that (1) The heat of solidification cannot be disregarded in the calculation of pavement temperature during a freezing process, and (2) The HMB model was able to reproduce the rise in salt (NaCl) concentration, the increase in the mass ice content and the reduction of the *BPN* value associated with the expansion of freezing of both fresh water and NaCl solution.

KEYWORDS

SLIDING RESISTANCE / ROAD SALTING / HEAT AND MASS TRANSFER / MASS ICE CONTENT / SALT CONCENTRATION / FREEZING

1. INTRODUCTION

Salting is the most popular anti-freezing measure for winter road management. The consumption of antifreeze agents has increased every year in Japan, although financial difficulties have been growing more serious. The concentration of salt solution on the road surface (henceforth, "salt concentration") after salting and road surface temperature are both important factors in salting operations.

However, neither the road surface temperature nor the salt concentration is a factor that indicates the level of danger in the road surface friction explicitly. Road sliding resistance, μ, is a more adequate and objective index than the road surface temperature and the salt concentration.

Therefore, better understanding the decrease in μ in addition to the time variations of the salt concentration and road surface temperature in the freezing process of liquid on the road surface is indispensable in order to prevent slip accidents due to road surface freezing and to reconcile safe winter traffic and reduction of antifreeze agents.

At present, salting operations are judged based on snow/ice (S/I) conditions on the road surface obtained from an ITV camera, patrol observation, various sensors and weather information. There is a strong need for a timely and appropriate manner of carrying out salting work using the ITS application and GIS data, but the timing of salting and the amount of antifreeze agents often have been entrusted to workers' judgment. The rate of salting may become excessive for purposes of giving priority to traffic safety.

One of the measures used to achieve optimal salting operations is that of developing a method of forecasting road freezing. Some attempts have been made to forecast road surface temperatures by statistical analysis and heat-balance analysis [1]-[7]. Recently, Numata et al. [8] proposed a salt concentration-forecasting model using a statistical approach. However, no optimal salting was systematized in their study.

We have been developing a coupled heat and mass balance model (HMB model) to forecast not only road surface temperature but also S/I conditions, which affect the μ value strongly. The HMB model is able to analyze the mass and volume balance equations of water, ice, and air components in the S/I layer on the road surface, so that the S/I conditions (fractions of snow density, snow height, mass ice content and water content) can be evaluated quantitatively. The heat transfer equations in the HMB contain some parameters that are changeable in terms of the mass ice content or the volumetric water content, such as thermal conductivity, albedo, transmissivity, emissivity of the S/I and the thermal resistance between the road surface and S/I. The advantage of the HMB model is that the freezing process of the S/I can be expressed by the decrease in the British Pendulum Number (*BPN*) with time.

In this study, a freezing experiment of sodium chloride (NaCl) solution on an asphalt pavement was carried out to examine the validity of the HMB model by comparison between calculated results and experimental ones regarding the time variations of pavement temperature, salt concentration, mass ice content and *BPN* value associated with the freezing expansion of NaCl solution and fresh water on the pavement (road) surface.

2. COUPLED HEAT AND MASS BALANCE MODEL

2.1. Freezing of NaCl solution

The freezing and melting processes of the ice-NaCl solution mixture (INSM) on the road surface follow the freezing point depression (FPD) shown in Figure 1. For example, the freezing process (point *a* → point *d*) in Figure 1 is explained as follows:

(i) The temperature of the INSM, T_s (= T_{sa}), at point *a* (no ice) is dropped to T_{sb} (freezing point, T_f, at point *b*) due to the net heat flux across the NaCl solution layer, Q_{net} (< 0),

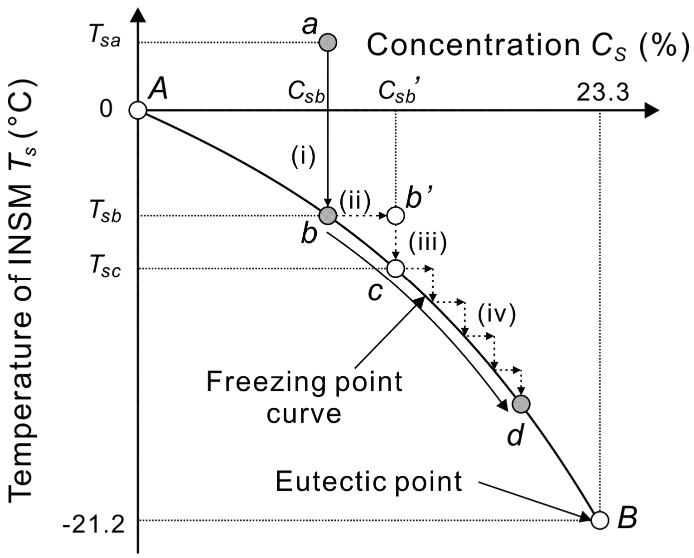

Figure 1 – Freezing process of NaCl solution on pavement surface

given by Eq. (12). There is no change in the salt concentration, C_s, on the route from point *a* to point *b*, i.e. $C_s = C_{sb}$.

(ii) After T_s reaches T_{sb}, negative Q_{net} is spent on freezing the NaCl solution. Thus, the fraction of water in the NaCl solution decreases and the remaining NaCl solution becomes more concentrated ($C_{sb} \rightarrow C_{sb}'$). In this process (point $b \rightarrow b'$), T_s remains at T_{sb}.

(iii) After C_s reaches C_{sb}', T_s drops further ($T_{sb} \rightarrow T_{sc}$) on the route from point *b*' to point *c*, where T_{sc} is the freezing point for C_{sb}'.

(iv) Thus, the freezing of NaCl solution progresses to point *d* along the FPD while repeating the rise in C_s and the depression of T_s.

Such stepwise freezing is improved by shortening the interval time for solving the heat and mass transfer equations discretized.

2.2. Assumptions and conditions applied to heat and mass transfer theory

In the present experiment, the following conditions and assumptions are applied to heat and mass balance theory to make it easier to evaluate the HMB model for NaCl solution.

(1) Solar radiation, snow/rain fall, road drainage and traffic related heats are ignored.
(2) NaCl solution does not flow out of the road surface (it stays on the road surface).
(3) Heat moves only in the vertical direction, and any horizontal movement of NaCl solution is ignored.

3. HEAT AND MASS TRANSFER THEORY

3.1. Volume and mass fractions of ice and NaCl

The volume of the INSM layer, V_s, is the total of the volume of ice, water and NaCl, V_i, V_w, and V_{sa}.

$$V_s = V_i + V_w + V_{sa} \tag{1}$$

C_s is given by

$$C_s = \frac{M_{sa}}{M_w + M_{sa}} \times 100 \tag{2}$$

where M_w and M_{sa} are the mass of the water and NaCl per unit area of pavement surface (henceforth, "unit area").

The volumetric water content, θ_w, and the volumetric ice content, θ_i, are given by

$$\theta_w = \frac{V_w}{V_s} \tag{3}$$

$$\theta_i = \frac{V_i}{V_s} \tag{4}$$

The mass ice content, Θ_i, is obtained by

$$\Theta_i = \frac{M_i}{M_w + M_i + M_{sa}} \tag{5}$$

where M_i is the mass of ice in the INSM layer per unit area.

3.2. Mass balance of water

Based on the assumptions and conditions in 2.2 and on the concept of heat transfer in the INSM layer shown in Figure 2, the mass balance of the water in the INSM layer is written as

$$\frac{\partial M_w}{\partial t} = -M_{wl} - M_{wi} \tag{6}$$

where M_{wl} is evaporation flux, M_{wi} is solidification flux and t is time.

M_{wl} is calculated by the following bulk equation,

$$M_{wl} = \alpha_{wl}\left(\rho_{vs} - \rho_{va}\right)\theta_w \tag{7}$$

where α_{wl} is the evaporation coefficient, ρ_{va} is the density of vapor in air and ρ_{vs} is the density of vapor on the INSM surface.

As C_s rises, ρ_{vs} is depressed as follows [9]:

$$\rho_{vs} = \rho_{vs0}\left(1 - 5.1 \times 10^{-6} C_s\right) \tag{8}$$

where ρ_{vs0} is the saturated vapor density on the freshwater surface.

When T_s is equal to an arbitrary freezing point, T_f, and $Q_{net} < 0$, M_{wi} is calculated by

$$M_{wi} = -\frac{1}{1000}\frac{Q_{net}}{q_{vt}} \tag{9}$$

where q_{vt} is the heat of solidification.

3.3. Mass balance of ice

The mass balance equation of the INSM layer is expressed by

$$\frac{\partial M_i}{\partial t} = M_{il} + M_{wi} \tag{10}$$

where M_{il} is sublimation flux and is given by

$$M_{il} = \alpha_{il}\left(\rho_{va} - \rho_{vs}\right)\theta_i \tag{11}$$

where α_{il} is the sublimation coefficient.

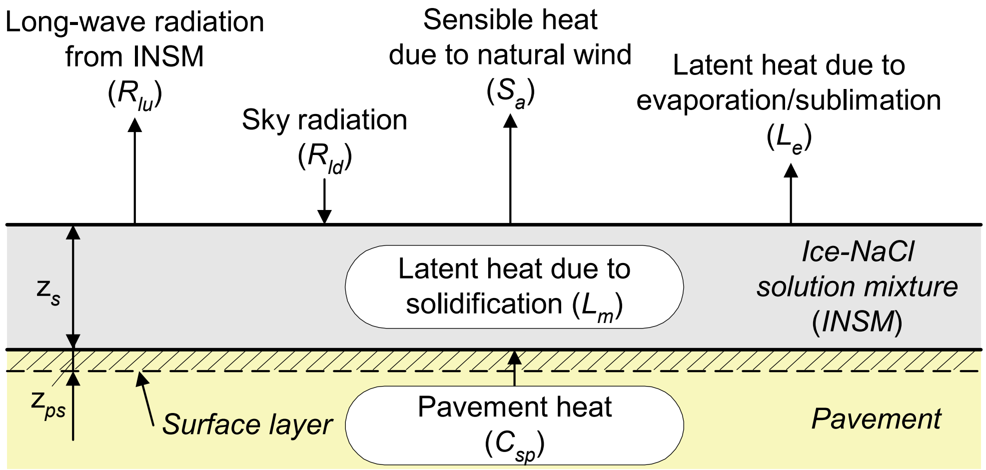

Figure 2 – Schematic view of heat balance of ice-NaCl solution mixture on pavement surface

3.4. Heat balance

The heat flux components acting on the INSM layer with a thickness of z_s are described in Figure 2:

$$\frac{\partial}{\partial t}\{(\rho c)_s z_s T_s\} = C_{sp} - R_{lu} + R_{ld} - S_a - L_e + L_m = Q_{net} \tag{12}$$

where $(\rho c)_s$ is the volumetric heat capacity of the INSM layer, C_{sp} is the pavement heat flux, R_{ld} is the sky radiation flux, R_{lu} is the upward long-wave radiation flux from the INSM surface, S_a is the sensible heat due to natural wind, L_e is the latent heat flux due to evaporation/sublimation and L_m is the latent heat flux due to solidification. $(\rho c)_s$ is given as the harmonic mean (weighted average) of the ice, water and NaCl in the INSM layer.

(a) Pavement heat flux

C_{sp} takes into account the contact heat resistance, R_c, at the interface between the INSM and the pavement surface and is calculated by

$$C_{sp} = \frac{1}{\dfrac{z_s/2}{\lambda_s} + \dfrac{z_{ps}/2}{\lambda_p} + R_c}\left(T_{ps} - T_s\right) \tag{13}$$

where λ_s is the thermal conductivity of the INSM, λ_p is the thermal conductivity of the pavement, z_{ps} is the thickness of the surface layer of the pavement and T_{ps} is the temperature of the surface layer of the pavement. R_c is calculated by the equation proposed by Fujimoto et al. [10]. λ_s is given as the harmonic mean of the thermal conductivity of the INSM.

(b) Long-wave radiation flux

R_{lu} is expressed by Stefan–Boltzmann's law:

$$R_{lu} = \varepsilon_s \sigma (T_s + 273.15)^4 \tag{14}$$

where σ is Stefan–Boltzmann's coefficient. ε_s is the emissivity of the INSM surface and is calculated by the following harmonic mean:

$$\varepsilon_s = \frac{\varepsilon_{ds}\theta_i + \varepsilon_w\theta_w}{\theta_i + \theta_w} \tag{15}$$

where ε_{ds} is the emissivity of ice and ε_w is the emissivity of water. R_{ld} in Eq. (12) is given as measurements.

(c) Sensible heat flux due to natural wind
S_a is given by Newton's law of cooling,

$$S_a = \alpha_{sa}(T_s - T_a) \tag{16}$$

where α_{sa} is the heat transfer coefficient between the INSM surface and the atmosphere.

(d) Latent heat flux due to evaporation/sublimation
L_e is calculated by using M_{wl} and M_{il} as follows:

$$L_e = M_{wl}q_e + M_{il}q_s \tag{17}$$

where q_e is the heat of vaporization and q_s is the heat of sublimation.

(e) Latent heat flux due to solidification
L_m is given by

$$L_m = M_{wi}q_m \tag{18}$$

where q_m is the heat of fusion.

4. FREEZING AND SLIDING RESISTANCE EXPERIMENTS

Figure 3 shows a schematic view of the freezing experiment in a low-temperature room (see the left half) and a photograph of the sliding resistance experiment (see the right half). The freezing expansion of fresh water and NaCl solution on a test piece of asphalt pavement was observed for six hours. T_s was measured with a thermo-couple inserted into the INSM layer 0.5 mm above the pavement surface (half the depth of the INSM layer). The pavement temperature, T_p, was measured with thermo-couples inserted in the pavement at different depths of 5, 10, 15, 25, 35 and 45 mm below the pavement surface. The ambient air temperature, T_a, and relative humidity, RH_a, were measured with a thermo-hygrometer at a height of 15 mm above the INSM surface. R_{ld} was measured with an infrared radiometer.

The pavement used in this experiment was a new 20 FH surface with a size of 300 (W) × 300 (L) × 50 mm (H). Its thermal conductivity was 1.4 W/m/K, its density was 2365 kg/m^3 and its specific heat was 0.86 kJ/kg/K. All aspects of the pavement were covered with a heat insulator with a thickness of 60 mm except the top surface (pavement surface). The experimental equipment was covered with a vinyl sheet to avoid sudden change of T_a and RH_a due to a body of cold air ventilation from the laboratory ceiling.

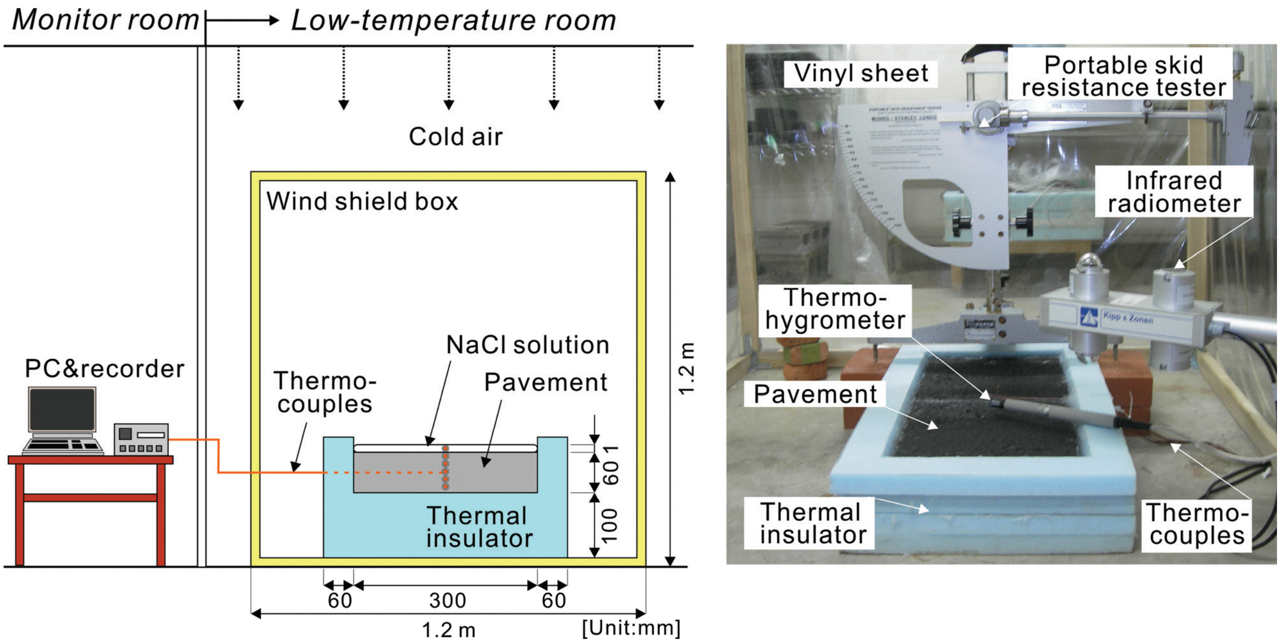

Figure 3 – Schematic view of freezing experiment and photograph of sliding resistance experiment

The experimental procedure was as follows:

(1) The pavement was put in a low-temperature room with an ambient air temperature of about 3°C.
(2) NaCl solution was supplied on the pavement surface to a depth of 1 mm.
(3) The ambient air temperature was controlled from 3°C to -12°C as soon as the experiment started.
(4) C_s was measured with a densimeter at two different positions on the pavement surface at intervals of 30 minutes.
(5) T_p, T_s, T_a, RH_a and R_{ld} were automatically downloaded to a computer via a data logger at intervals of 1 minute.

The sliding resistance experiment was conducted simultaneously and the output was given as the *BPN* value. The *BPN* measurement was conducted every 30 minutes.

The experiment was classified into two case types. One was the freezing of fresh water (Case 0) and the other was the freezing of NaCl solution (the initial C_s [= C_{s0}] was 2% [Case C2], 4% [Case C4] and 8% [Case C8]).

5. RESULTS AND DISCUSSIONS

5.1. Temperatures of the ice-fresh water mixture (IFWM), INSM and pavement

(a) Fresh water

Figure 4 shows T_a, T_s and T_p-profiles at different t for Case 0. The solid and the dashed lines in Figure 4 represent numerical results including and excluding the heat of solidification, respectively. The former is termed Cal-A and the latter is termed Cal-U. T_a was 2.4°C initially and then fell to -10.4°C after beginning the experiment (t = 270 minutes). Initial T_s and T_p ranged from 3.6°C to 4.0°C. T_s fell to 0°C at t = 120 minutes, associated

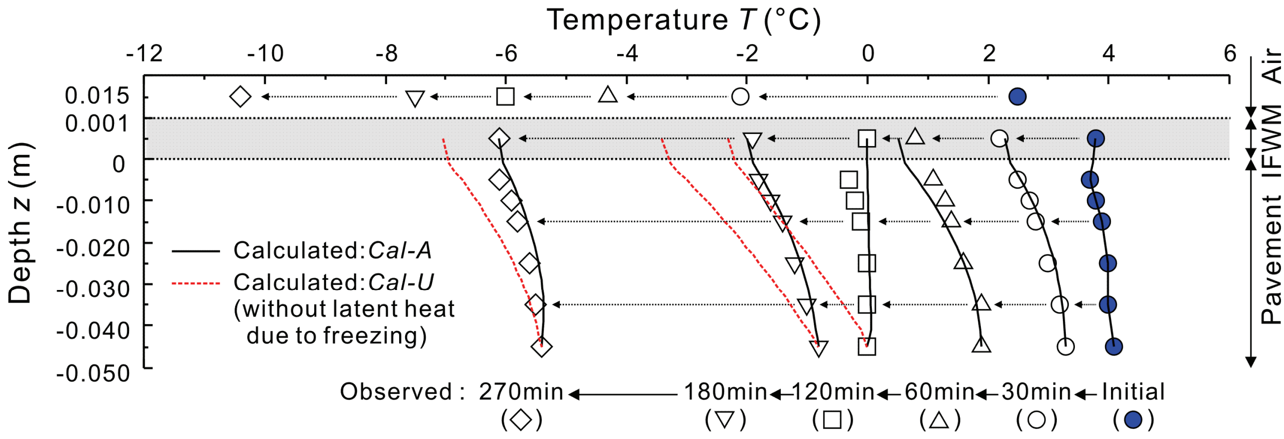

Figure 4 – Time variations of T_a, T_s and T_p-profiles
(Case 0: Fresh water)

with the fall in T_a. T_p decreased monotonously from the pavement bottom to the surface, except near the pavement surface of the T_p-profile at t = 120 minutes. This temperature inversion ($T_p < T_s$) may be caused by the rise in T_s due to the heat of solidification, although T_P was below the freezing point due to overcooling of the IFWM. Since T_s was lower than the freezing point at t = 180 minutes, it was inferred that the IFWM was completely frozen by that point in time.

Cal-A reproduced satisfactorily the time variation of the T_p-profile measured, while Cal-U underestimated T_p (i.e., it was calculated lower than the observed T_p). It is seen that the heat of solidification cannot be disregarded in calculation of fresh water freezing on the road surface.

(b) NaCl solution

Figure 5 (a), (b) and (c) show the T_a, T_s and T_p-profiles at different t for Case C2, Case C4 and Case C8, respectively. The solid line in Figure 5 represents the T_p calculated by Cal-A. The result of Cal-U (dashed line) is shown only for Case C2. First, the results of Case C2 are described. T_p fell monotonously from the pavement surface toward the bottom, associated with thermal conduction the same as in Case 0. The absolute value of the temperature gradient, $|dT_p/dz|$, near the pavement surface at t = 120 minutes was smaller than that at t = 30 or 60 minutes. It is inferred that T_s reached T_f (= -1°C) for C_{so} = 2% at 60 < t ≤ 120 minutes and that the heat of solidification was injected in the NaCl solution. T_s fell and C_s rose as soon as the freezing of the NaCl solution started.

Next, the results of Case C4 are described. The time variation of T_p-profiles was the same as that for Case C2. The temperature inversion ($T_p < T_s$) was observed at t = 180 minutes and occurred later by comparison with that for Case C2.

Finally, the results of Case C8 are described. The rate of decline in T_s and T_p with time was fastest in this case because the heat of solidification did not occur as long as T_s did not fall to -6°C, which is T_f for C_{s0} = 8%.

Thus it can be seen that the heat of solidification cannot be disregarded in calculation of freezing of NaCl solution either.

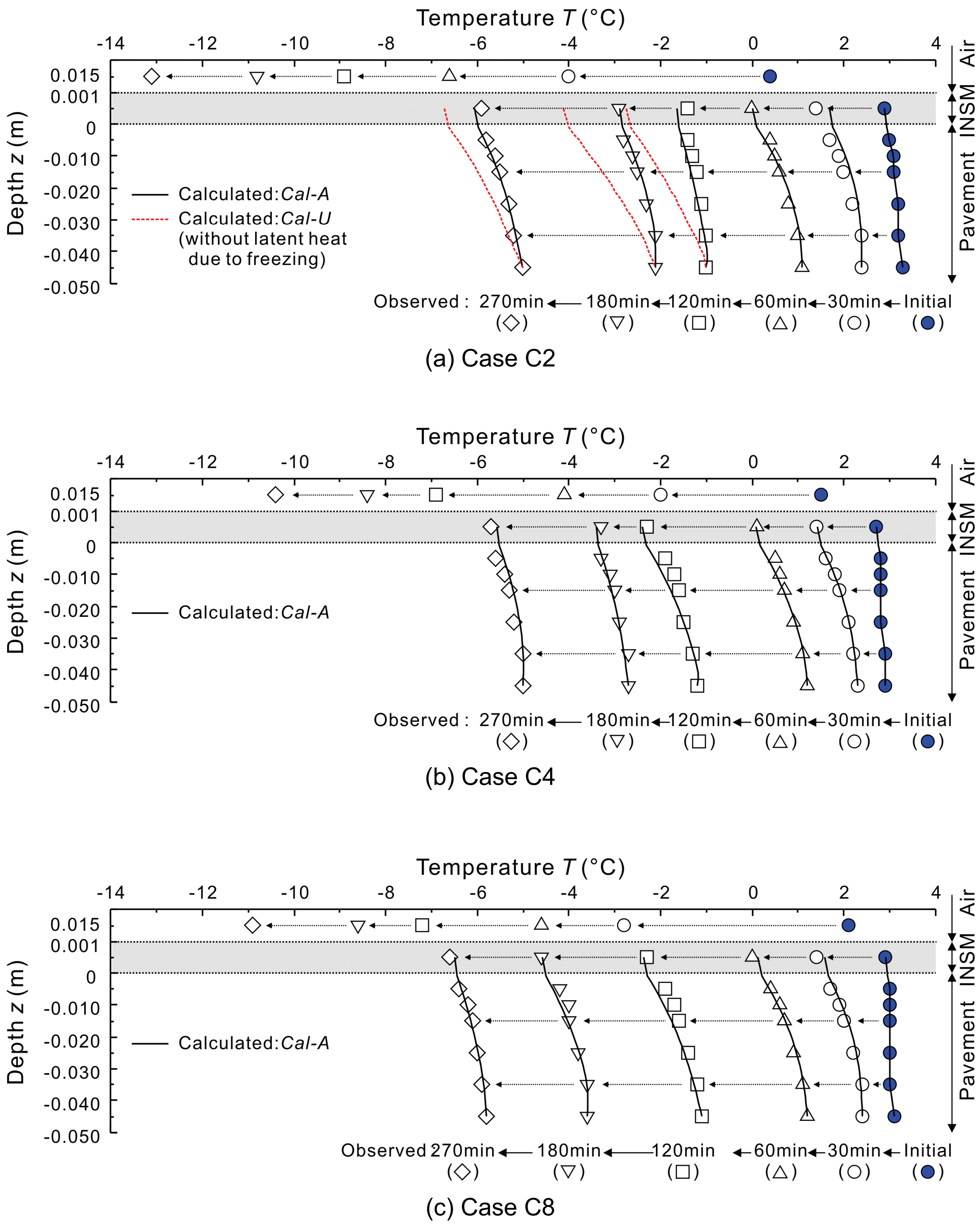

Figure 5 – Time variations of T_a, T_s and T_p-profiles
(NaCl solution)

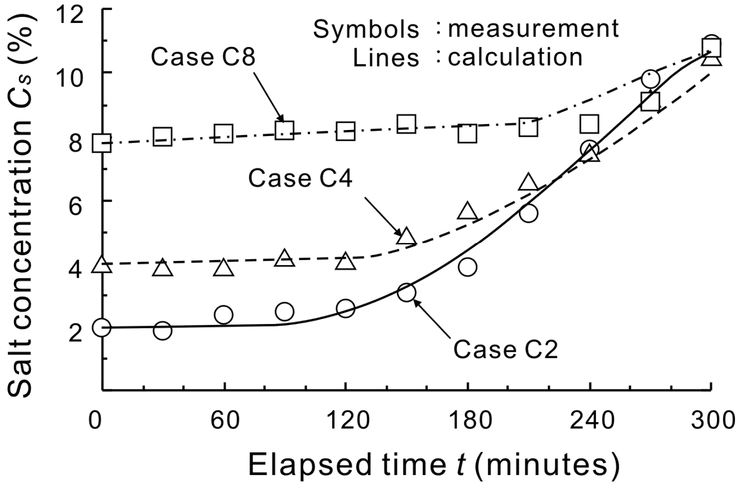

Figure 6 – Time variation of salt concentration C_s

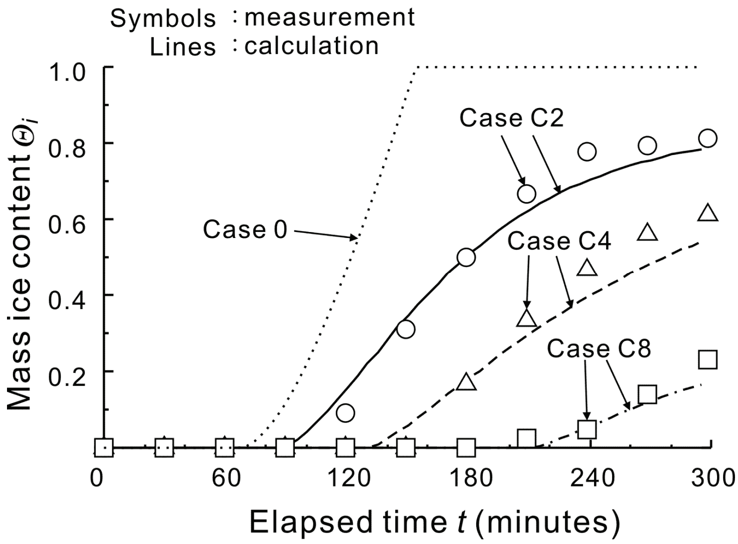

Figure 7 – Time variation of mass ice content Θ_i

5.2. Salt concentration

Figure 6 shows the time variation of C_s, $C_s(t)$, for C_{s0} = 2%, 4% and 8%. The calculated $C_s(t)$ shown in a solid line and two kinds of dashed lines were in good agreement with the experimental results. C_s rose at t = 90, 120 and 220 minutes for Case C2, Case C4 and Case C8, respectively. The rate of increase in C_s over time increased for Case C2, Case C4 and Case C8, in that order.

5.3. Mass ice content

Figure 7 shows the time variation of Θ_i. The increase in Θ_i with time appeared first in Case C2, next in Case C4 and then in Case C8. The rate of increase in Θ_i, $d\Theta_i/dt$, rose when C_{s0} was low and then fell with time for all cases. The commencement of freezing for Case 0 was earlier than that for Case C2, although this was a judgment based on numerical results.

The computational results were in good agreement with the experimental ones.

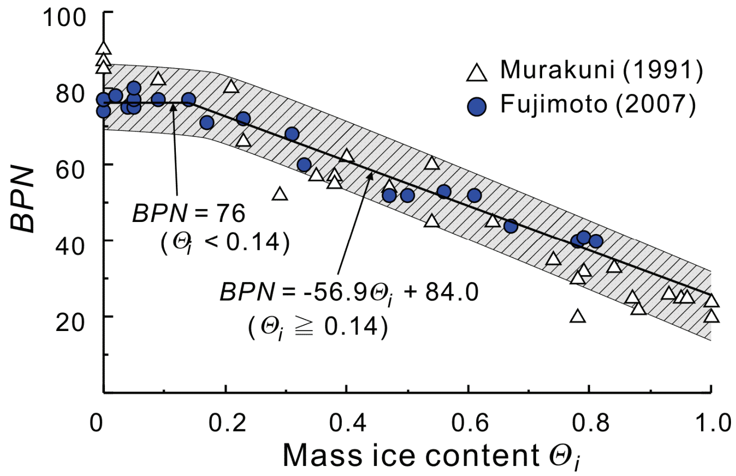

Figure 8 – Relationship between *BPN* value and Θ_i

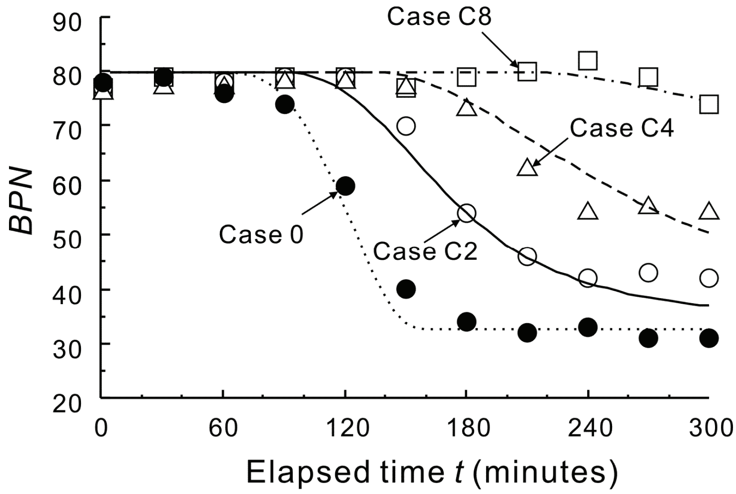

Figure 9 – Time variation of *BPN* value

5.4. Skid resistance

Figure 8 shows the relationship between the *BPN* value and Θ_i. The data measured by Murakuni [11] also is plotted in Figure 8, using triangles. The *BPN* value for $\Theta_i < 0.14$ was 76 *BPN* and was the same as the level for a wet road surface. The *BPN* value, however, decreased with Θ_i for $\Theta_i > 0.14$. There was little difference in both *BPN* - Θ_i relations for $0.1 \le \Theta_i \le 0.8$. The *BPN* value is approximated in terms of Θ_i as follows:

$$BPN = \begin{cases} 76.0 & (\Theta_i < 0.14) \\ -56.9\Theta_i + 84.0 & (\Theta_i \ge 0.14) \end{cases} \tag{19}$$

Figure 9 shows the time variation of the *BPN* value for Case 0, Case C2, Case C4 and Case C8, respectively. The commencement of the decrease in the *BPN* value was delayed and the rate of decrease in *BPN*, $dBPN/dt$, became smaller as C_{s0} rose. The time variation of the computed *BPN* value was in good agreement with the observed one for all cases.

6. CONCLUSIONS

We have developed a coupled heat and mass balance model (HMB model) for determining the skid resistance *BPN* for snow/ice (S/I) conditions on a road surface. The reliability of the HMB model was examined by comparison with the pavement temperature, the temperature and mass ice content of the ice-NaCl solution (or ice-fresh water) mixture on the road surface, the salt concentration and the *BPN* value that were obtained from a laboratory experiment.

The main conclusions drawn in the present study are as follows:

(1) The heat of solidification cannot be disregarded for the calculation of pavement temperature during a freezing process.

(2) The HMB model was able to reproduce the rise in salt (NaCl) concentration, the increase in the mass ice content and the reduction of the skid resistance with time associated with the expansion of freezing of both fresh water and NaCl solution.

REFERENCES

[1] B.H. Sass (1992). A numerical model for prediction of road temperature and ice. *The Journal of Applied Meteorology*, 31, 1499-1506.

[2] J. Shao & P.J. Lister (1996). An automated nowcasting model of road surface temperature and state for winter road maintenance. *The Journal of Applied Meteorology*, 35, 1352-1361.

[3] K. Yamakawa et al. (1996). Prediction of the slipperiness of a road surface in winter using a Neural-Kalman filter, *Proceedings of 1996 Cold Region Technology Conference*, 12, 189-194.

[4] T.V. Samodurova (2000). Models for short-term road ice formation forecast, *International Road Weather Conference*, 10.

[5] L. Chapman & J.E. Thornes (2002). A blueprint for 21st century road ice prediction, *International Road Weather Conference*, 11.

[6] E. Pasero et al. (2004). Neural Meteorological Forecast, *International Road Weather Conference*, 12.

[7] B. Morstad et al. (2004). Thermal model for contaminated snow on pavement, *Proceedings of the Fifth International Conference on Snow Engineering*, 5, 33-38.

[8] M. Numata et al. (2006). The report of the evaluation which make sprinkling of the road surface freezing prevention medicine proper. *Proceedings of 2006 Cold Region Technology Conference*, 22, 218-223.

[9] Chao HE et al. (2003). Heat, moisture and salt movement in a soil containing a salt accumulated layer due to watering and evaporation, *Journal of Hydraulic, Coastal and Environmental Engineering*, 747/II-65, 15-28.

[10] A. Fujimoto et al. (2007). Thermal contact resistance between snow/ice layer and pavement surface, *Journal of Materials, Concrete Structures and Pavements*, 63, 1, 156-165.

[11] M. Murakuni (1991). Relation between the phase change occurring within the temperature range below the freezing point of a chemical solution spread on road-surface and the value of skid resistance, Expressways and Automobiles, 34, 2, 20-26.